Geomechanics and Engineering, *Vol. 18, No. 2 (2019) 205-213*
DOI: https://doi.org/10.12989/gae.2019.18.2.205

Study on the distribution law and influencing factors of pressure field distribution before exploitation in heavy oilfield

Xing Zhang[1a], Ting T. Jiang*[2], Jian H. Zhang[2b], Bo Li[3c], Yu B. Li[2d], Chun Y. Zhang[2e], Bing B. Xu[2f] and Peng Qi[2g]

[1]*Research Institute of Petroleum Engineering Technology, Shengli Oilfield, SINOPEC, Xisan Road No. 306, Dongying, 257000, Shandong, People's Republic of China*
[2]*Hubei Province Key Laboratory of Processing of Mineral Resources and Environment, School of Resource and Environmental Engineering, Wuhan University of Technology, Luoshi road No.122, Wuhan 430070, Hubei, People's Republic of China*
[3]*Key Laboratory Geotechnical Mechanics and Engineering of the Mechanics and Engineering of the Minister of Water Resources, Changjiang River Scientific Research Institute, Huangpu Road No.23, Wuhan, 430070, Hubei, People's Republic of China*

(Received November 5, 2018, Revised May 22, 2019, Accepted May 28, 2019)

Abstract. A calculation model of reservoir pressure field distribution around multiple production wells in a heavy oil reservoir is established, which can overcome the unreasonable uniform-pressure value calculated by the traditional mathematical model in the multiwell mining areas. A calculating program is developed based on the deduced equations by using Visual Basic computer language. Based on the proposed mathematical model, the effects of drainage rate and formation permeability on the distribution of reservoir pressure are studied. Results show that the reservoir pressure drops most at the wellbore. The farther the distance away from the borehole, the sparser the isobaric lines distribute. Increasing drainage rate results in decreasing reservoir pressure and bottom-hole pressure, especially the latter. The permeability has a significant effect on bottom hole pressure. The study provides a reference basis for studying the dynamic pressure field distribution before thermal recovery technology in heavy oilfield and optimizing construction parameters.

Keywords: thermal recovery; reservoir pressure; stress sensitivity; exploitation; numerical simulation

1. Introduction

Thermal recovery technology is an effective means to improve the fluidity of heavy oil reservoir and enhance recovery efficiency (Mahdavi *et al*. 2018, Kim *et al*. 2016, Zhang *et al*. 2019). However, the formation pressure must be reduced before thermal recovery in heavy oilfield (Deshamukhya *et al*. 2019, Wang *et al*. 2018a, Wang *et al*. 2018*b*, Shalaby *et al*. 2017). The flows of fluid in heavy oil reservoir are complicated because of the existence of multiple wells, which causes the complexity of the reservoir pressure distribution (Cavicchio *et al*. 2018, Bader *et al*. 2018, Wang *et al*. 2019, Ziabakhsh-Ganji *et al*. 2017). Therefore, it is of great significance to fully understand the dynamic change process of reservoir pressure in heavy oilfield (Wang *et al*. 2018c, Kumar *et al*. 2017, Riazi *et al*. 2015, Wang *et al*. 2018d). Several theoretical and experimental studies have been carried out in the past to investigate the reservoir pressure distribution characteristics, and analyze multiple parameters on the reservoir pressure in heavy oil reservoir.

Taghizadeh (2018) considered the effective stress, porosity and permeability were affected by the multi-physical coupling of thermal, hydraulic and mechanical processes in heavy oil reservoir, which resulted in a complex interaction of geomechanical effects and multiphase flow in the porous media. Rostami (2017) found that the oil viscosity reduction and oil swelling were the most influential mechanisms of enhanced heavy oil recovery. Doranehgard (2018) studied the process of hot water injection into oil reservoirs with temperature dependent viscosity and proposed the relative permeability functions. Meanwhile, he used an improved streamline approach to enhance computational performance. Osgouei (2018) carried out an experimental study to investigate the role of various clay and non-clay minerals present in heavy oil reservoir formations on steam distillation process. Oskouel (2017) developed a new multi-component kinetic model to simulate the non-equilibrium gas ex-solution

*Corresponding author, Ph.D.
E-mail: jiangtingting104@163.com
[a]Professor
E-mail: zhangxing.slyt@sinopec.com
[b]Professor
E-mail: zjhwut@sina.com
[c]Professor
E-mail: auliso2004@126.com
[d]Professor
E-mail: Yubiao.li@whut.edu.cn
[e]Professor
E-mail: zcl2722@163.com
[f]Master Student
E-mail: 18302925673@163.com
[g]Master Student
E-mail: 18681263036@163.com

ISSN: 2005-307X (Print), 2092-6219 (Online)

process in heavy oil. The new model revealed that there must be a minimum excess concentration of the dissolved gas in the oil phase to drive the bubble formation reaction. Salmo (2017) pointed out that saturation-induced crossflow into water channels at homogeneous permeability was found to be strongly affected by wettability, viscosity ratio (oil/water), and the width of water channels. Jahani-Keleshteri and Bahadori (2017) thought that the viscosity had great effect on the fluid flow characteristic and oil recovery prediction. Hasanvand (2017) performed a series of laboratory experiments on heavy oil sample to determine its kinetic and thermodynamic properties and found that the particle size and distribution of oil were sensitive to temperature and pressure. Kumar and Okuno (2015) presented a new method for reservoir fluid characterization that directly perturbed the attraction and covolume parameters of pseudo components from the n-alkanes' values. Arciniegas and Babadagli (2014) classified the characteristics of asphaltene in terms of the shape, size, and amount for different oil/solvent types, pressure, and temperature.

However, these achievements mentioned above were mainly based on the assumption that the reservoir pressure changed regularly. The research object of this paper is the heavy oil reservoir of Gudao oilfield in Dongying city of Shandong province in China. The whole area is about 1 km^2 and fifteen oil wells are located in the area based on field measured data. The area cannot be viewed as an infinite region. The reducing pressure process is dynamic before thermal mining. The available models may not be suitable for modeling the oil reservoir in Gudao oilfield. Moreover, studies about the effects of construction and geological parameters on dynamic pressure distribution in heavy oil reservoir are rare.

The motivation of this paper is to better understand the dynamic change characteristics of the reservoir pressure during drainage and to study the implementation and the formation factors influencing the reservoir pressure in the heavy oilfield. Based on the the potential superposition principle, an reservoir pressure distribution model of the heavy oil reservoir was built. The initial conditions, the auxiliary equations and the boundary conditions were used to solve the model to realize the numerical simulation of reservoir pressure distribution pattern. The proposed model was used to analyse the influence of drainage rate and formation permeability on the reservoir pressure. Research results provide a reference basis for studying the dynamic pressure field distribution before thermal recovery technology in heavy oilfield and optimizing construction parameters.

2. Reservoir pressure distribution model and numerical simulation

2.1 Distribution of reservoir pressure field around multiple production wells

When multiple wells work simultaneously in the reservoir, any change in the working state of a well will inevitably result in the change of the output or the flowing bottomhole pressure of the other wells. This phenomenon is called the well interference phenomenon (Amirian *et al.* 2018a, b, 2015). As long as there are more than a well in the oil layer, there will be interference between wells which cannot be inevitable. Before the change of the well operating state, multiple wells are in a stable state. The energy supply and consumption in the entire reservoir are in a temporary equilibrium. The change in the working state of any well will destroy the original energy balance, causing the change of the entire seepage field, so the pressure in the strata will be redistributed.

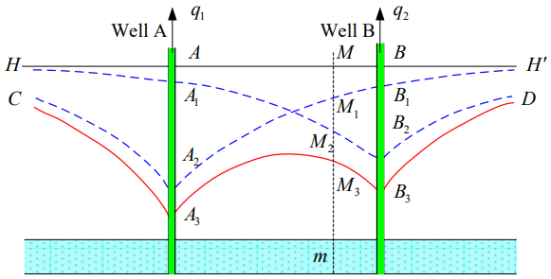

Fig. 1 The pressure distribution diagram of two interferential wells

The paper has established a reservoir pressure distribution model based on two production wells. We assume that the oil reservoir is a circle with the radius of R. The two wells work together with the output q_1 and q_2, respectively. When the oil layer has not been developed yet, all the points in the stratum are the original formation pressure. Its value is expressed by solid line *H-H'* which is shown in Fig. 1. We assume that only Well A is in producing and the output is q_1. It consumes the formation energy to form the pressure drop funnel as shown by dotted line A_2B_1. The bottom hole pressure drop of Well A is AA_2, which leads to a pressure drop of BB_2 near the bottom of Well B. Meanwhile, the pressure drop near Well B forms an extra pressure drop (AA_1) of Well A. When both Well A and Well B produce together with the original output q_1 and q_2, the bottom-hole pressure of Well A drops to the dot A_3. And that A_2A_3 is equal to AA_1. For the whole stratum, the pressure distribution of each point in the formation is distributed by the curve $CA_3M_3B_3D$ when the two wells produce at the same time.

The substance of well interference is the rebalance of energy in the stratum. The magnitude of energy is expressed by pressure, so the final result is the pressure redistribution in the oil reservoir. This redistribution is based on the principle of the pressure drop superposition, which means the pressure drop of any point is the algebraic sum of the pressure drop when each well works alone.

In oil reservoir, fluid elements flow to the point sink. If we draw a circle with the center of the circle located at the point sink, the flow rate of plane radial seepage is

$$q = \frac{2\pi Krh}{\mu}\frac{dp}{dr} \tag{1}$$

where K is the permeability; r is the radius of the circle; h stands for the thickness of the reservoir; μ is the fluid viscosity.

$$\frac{q_h}{2\pi r}=\frac{d\phi}{dr} \tag{2}$$

where q_h is the flow rate of unit-thickness reservoir, $q_h=q/h$; ϕ is velocity potential, $\phi=Kp/\mu$.

Separating variables and doing integration, the potential at any point in a plane is shown as below (Inarrea *et al*. 2019, Kurek *et al*. 2018)

$$\phi=\frac{q_h}{2\pi}\ln r+C \tag{3}$$

where C is the integration constant confirmed by boundary conditions.

Because of the additivity property of potential, the potential at any point is shown as follows when multiple wells work simultaneously.

$$\phi=\sum_{i=1}^{n}\pm\frac{q_{hi}}{2\pi}\ln r_i+C \tag{4}$$

where r_i is the distance from any point to the wellbore.

The potential at the supply boundary is (Jiang *et al.* 2017)

$$\phi_e=\sum_{i=1}^{n}\pm\frac{q_{hi}}{2\pi}\ln r_e+C \tag{5}$$

where ϕ_e is the potential at the supply boundary; r_e is the supply radius.

Subtract Eq. (5) from Eq. (4), the pore pressure at any point is shown as below

$$p=p_e-\frac{\mu}{2\pi Kh}\sum_{i=1}^{n}\pm q_i\ln\frac{r_e}{r_i} \tag{6}$$

The pore pressure at the bottom hole is

$$p_{wfj}=p_e-\frac{\mu\varphi^{\Theta}}{2\pi Kh}\left(q_j\ln\frac{r_e}{r_w}+\sum_{\substack{i=1\\ i\neq j}}^{n}\pm q_i\ln\frac{r_e}{r_i}\right) \tag{7}$$

$$i=1,\cdots,n;\ j=1,\cdots,n$$

where p_e is the pore pressure at the supply boundary; r_w is the radius of oil well; φ is the reservoir porosity; Θ stands for the reservoir porosity coefficient.

2.2 Initial conditions and auxiliary equations

At the initial stage of development, the reservoir pressure can be expressed as

$$P(x,y,z,t=0)=f(x,y,z) \tag{8}$$

where $f(x,y,z)$ is the known function of the reservoir pressure.

The linear flow in porous media is consistent with Darcy's law, which reflects the relationship between pressure gradient and fluid flow velocity.

$$V_s=-\frac{k}{\mu}\left(\frac{\partial p}{\partial s}-\rho g\sin\theta\right) \tag{9}$$

where V_s the is seepage velocity, μ is fluid viscosity, k is the permeability, ρ is the fluid density, θ is the included angle between horizontal plane and the positive direction of V_s.

When the fluid flows in the porous media, the fluid mass will neither increase nor decrease. According to the mass conservation law, the continuity equation can be written as

$$\begin{aligned}&\Delta t\left[-\oiint_{\sigma}\rho\left|\vec{V}\right|\cos(\vec{n},\vec{V})dA+\iiint_{\Sigma}G(x,y,z,t)dV\right]\\&=\left(\iiint_{\Sigma}\phi\rho dV\right)_{t+\Delta t}-\left(\iiint_{\Sigma}\phi\rho dV\right)_{t}\end{aligned} \tag{10}$$

where $\sum$ is volume element, dV stands for the volume of the volume element, σ is the boundary, t is the time, $G(x,y,z,t)$ is the intensity of the source or sink.

2.3 Boundary conditions

2.3.1 Internal boundary

The flow pressure in the wellbore can be thought as a constant when the oil well parameters are determined, such as the diameter and the length of the wellbore. The internal boundary conditions are

$$P(0,0,0,t)=P_u(R_z,R_l)\ \ (t>0) \tag{11}$$

where P_u is the flowing pressure in the wellbore, R_z is effective radius controlled by a single well, R_l stands for wellbore effective length.

2.3.2 External boundary

The constant pressure of the boundary is often defined as the first boundary condition. The pressure distribution at any point on the outer boundary $\Xi 1$ can be written as

$$P(x,y,z,t)\big|_{\Xi 1}=P_a(x,y,z,t)\ \ (t>0) \tag{12}$$

The constant flow rate of the boundary is called the second boundary condition. It is thought that the boundary $\Xi 2$ is closed and that no fluid passes through it. The boundary expressions are as follows

$$\frac{\partial p(x,y,z,t)}{\partial n}\Big|_{\Xi 2}=0\ \ (t>0) \tag{13}$$

where p_a (x,y,z,t) is stress function, $\left.\frac{\partial p}{\partial n}\right|_{\Xi 2}$ stands for the derivative of the boundary pressure along the outer normal direction of boundary $\Xi 2$, p_f is the initial stress in the reservoir.

2.4 Numerical solution

To improve the efficiency of the proposed mathematical model, we develop the calculating program by using the Visual basic computer language. The program is named "Reservoir pressure distribution software for multiple well area in heavy oilfield", and is shortened to ResPreDist. Fig. 2 presents the flowchart of ResPreDist simulator. It is composed of four parts, e.g., data input, mathematical

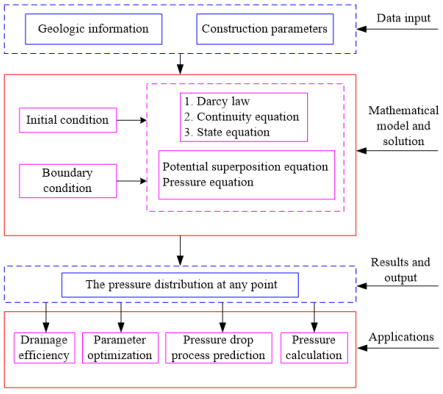

Fig. 2 Flowchart for ResPreDist simulator

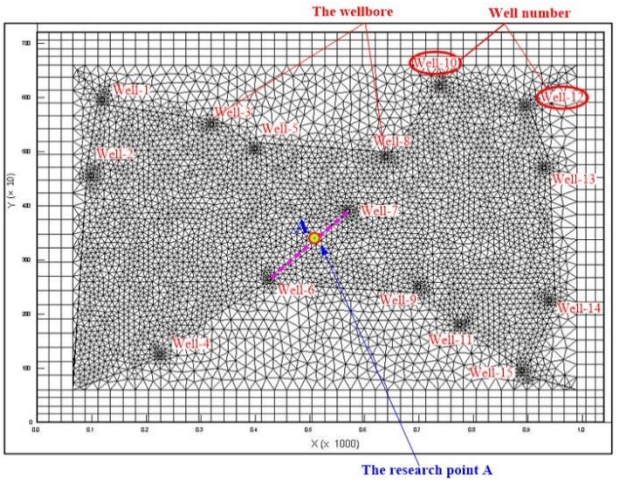

Fig. 3 Finite element grid model of the test site of Gudao oil field

model and solution, results and output, and applications. First, the input data is composed by two parts. One is the data obtained by geologic information, which include the reservoir pressure, thickness, permeability, the whole area, length and width of the teat region. The other one are the construction parameters, such as the viscosity and density of fluid, the well diameter, the liquid amount and the drainage speed. They are identified automatically by the simulator and are assigned to the corresponding array for the later calculations. The pressure distribution of any point in the reservoir field can be obtained during the solution of the mathematical model. In the model solving process, the boundary conditions including internal boundary and external boundary are important auxiliary equations. Then, these calculation results can be output with different types, e.g., figure, table and text. Lastly, we can use above calculating results to evaluate the drainage efficiency and optimize the construction parameter, to predict the pressure drop process of the whole area, and to calculate the pressure value for the wellbore.

By using ResPreDist, the test block of heavy oil reservoir including fifteen oil wells in Dongying city are simulated, and the effects of drainage rate and formation permeability on reservoir pressure are investigated. The construction parameter of the test block can be optimized based on the calculating results. The field data can be monitored to verify the accuracy and reliability of the mathematical model.

3. Simulation results and analysis

Gudao oilfield in Dongying city adopted water flooding formerly in the mining. In order to increase oil production, it is necessary to convert from conventional waterflooding to heat recovery steam injection of heavy oil in Gudao oilfield. According to process requirements, the reservoir pressure must be reduced to a certain range before thermal recovery technology. So we stopped the water flooding from injection wells and kept the production wells continuing to produce to reduce the reservoir pressure. It can make the formation reach a certain deficit, so as to achieve reducing the reservoir pressure. The average thickness of the oil reservoir is 11.8 m. The area of the test site of Gudao oil field is about 1km×1km and fifteen oil

Table 1 Simulation parameters of reservoir pressure field

No.	Items	Unit	Value
1	Well number		15
2	Reservoir pressure	MPa	9.6
3	Permeability	mD	1560
4	Porosity	%	6.4
5	Reservoir thickness	m	11.8
6	Fluid viscosity	mPa·s	1
7	Area of the test region	km^2	1
8	Total liquid amount	m^3	2780000
9	Length of the test region	m	1000
10	Width of the test region	m	1000
11	Fluid density	kg/m^3	1000
12	The well diameter	mm	139.7
13	The well effective length	m	11.5
14	The well effective radius	m	126
15	Drainage speed of a single well	m^3/d	96

wells are located in the area. The wellbore is very small relative to the whole region, so the fluid flow can be assumed as horizontal radial seepage. Based on the field measured data, the content of oil in produced liquid is low. So the parameters of water can be used in numerical simulation.

According to the reservoir pressure distribution model established in Section 2, the numerical simulation model is built based on the in-situ data of test site in Gudao oilfield. The numerical model is shown in Fig. 3. It is a square with both side length of 1000 m and the area of 1000 m^2. The directions of X, Y axes represent the length and the width of the test area, respectively. In this area, there are fifteen oil wells which are marked by the well number. The model is modeled in proportion of 1:2000 with 5398 nodes and 9401 elements. Based on field measured data, the reservoir pressure drops 1MPa if 0.2 million m^3 of water and oil has been produced. Total liquid amount of the test site is 2.78 million m^3 and the reservoir pressure is 9.6 MPa. It would

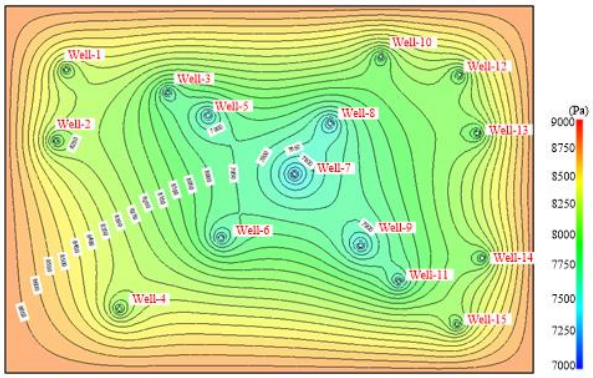

(a) 60 days

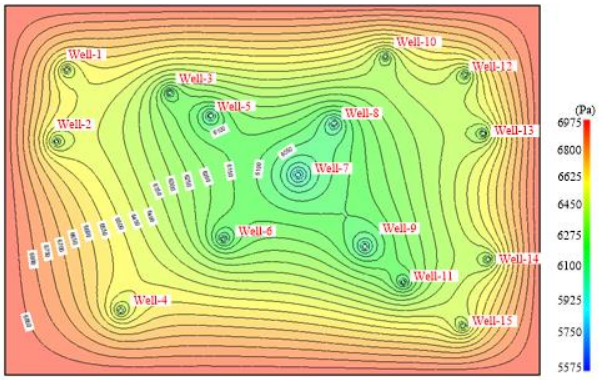

(b) 180 days

Fig. 4 The diagram of reservoir pressure distribution

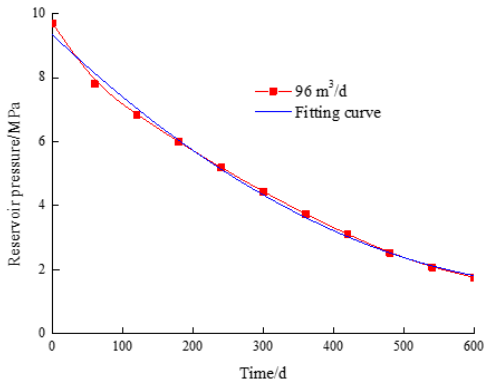

Fig. 5 The curve of reservoir pressure over time

meet the technological requirements of steam-injected thermodynamic oil exploitation when the production reaches 1 million cubic meters. In order to show the model diagram more clearly, different proportions of X axis and Y axis are used. Table 1 lists the parameters used in the numerical simulation.

3.1 Evaluation of pressure drop in heavy oilfield

Fig. 4 presents the reservoir pressure distribution in X-Y plane. The reservoir pressure drop is a dynamic process. The pressure keeps falling with the fluid in the formation continues to be produced. In the figure, the closed lines colored in black are isobars with the pressure values marked on them. The area between Well-7 and Well-6 has lower reservoir pressure. The further away from the area, the higher the reservoir pressure is. The pressure decreases faster near the bottom hole, this is because the seepage area is smaller and the seepage resistance is greater. The influence reduces gradually with increasing distance from the bottom of the well. The change in reservoir pressure also becomes slow, which are rendered in X-Y plane: the farther the distance away from the borehole, the sparser the isobaric lines distribute. The point that the reservoir pressure drops the fastest is close to Well-7. So the casing pipe of Well-7 suffers the greatest force. We should closely monitor the drainage rate to prevent the casing damage. Fig. 4(a) and Fig. 4(b) are the reservoir pressure distribution plots after the discharge for 60 days and 180 days respectively. After 180 days of production, the reservoir pressure decreases dramatically. And the pressure difference of the whole research region decreases greatly.

On the basis of above analyses, it is shown that the area between Well-7 and Well-6 has the lower reservoir pressure. So in order to better study the influence law on reservoir pressure, the point which is 7.1 m far from Well-7 is studied as a key research object. The location-specific information of the point A is shown in Fig. 3, which locates the line between Well-7 and Well-6. Fig. 5 shows the relation between reservoir pressure and time of point A. As is shown in the graph, the pressure decreases exponentially with time at the condition of drainage speed is 96 m^3/d. In the early stage, the descent velocity is faster while it becomes slow in the middle and late stage. The corresponding fitting curve of reservoir pressure and time is also shown in Fig. 5 which is marked by blue line, and the relationship equation is shown below.

$$P_R = 1.38047\mathrm{E} - 5T^2 - 0.02083T + 9.34545 \quad (14)$$

where P_R is the reservoir pressure, MPa; T is the time, d.

3.2 Parametric research on reservoir pressure

By using the numerical simulation model established in Section 3.1, the effects of multiple parameters including drainage rate and formation permeability on reservoir pressure distribution are studied.

3.2.1 Effect of drainage rate on reservoir pressure

To investigate the effects of the drainage rate of a single well on the reservoir pressure, the drainage rate is taken as 36, 48, 60, 72, 84, 96, 120, 156 and 180 m^3/d respectively. Because the reservoir pressure is the most sensitive in the early stage of reservoir drainage, the mining time is set as a constant to study the impact of drainage rate on reservoir pressure. The other parameters used in the simulations are valued as listed in Table 1.

Fig. 6 shows the reservoir pressure distribution of different drainage rates (72 m^3/d and 180 m^3/d) and the production time is 45 days. With the increase of the drainage rate, the total amount of drainage also increases by a large margin in the same construction time. As the liquid is discharged from the stratum, the reservoir pressure decreases gradually. The reservoir has greater pressure losses leading to faster pressure drop when the drainage rate is higher. In the actual construction process, we should avoid too fast drainage rate. It may result in the exploitation

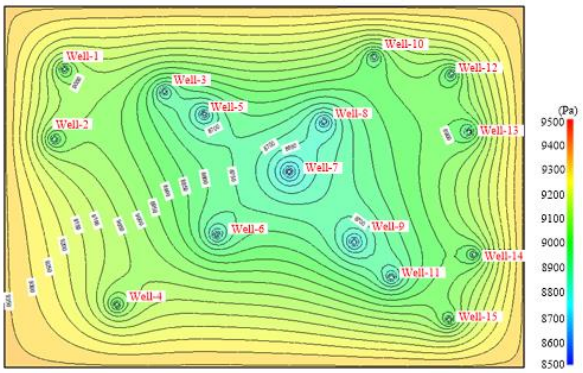

(a) Drainage rate is 72 m^3/d

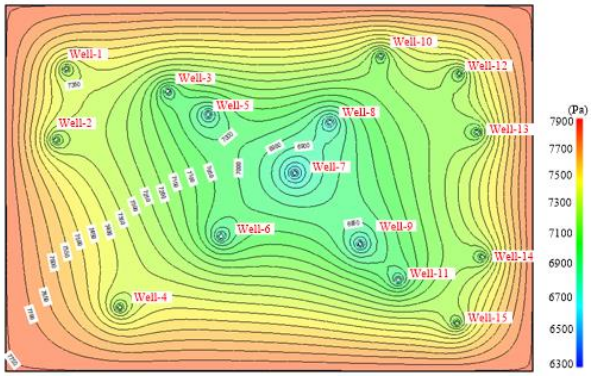

(b) Drainage rate is 180 m^3/d

Fig. 6 The reservoir pressure distribution diagrams of different drainage rates after 45 days production

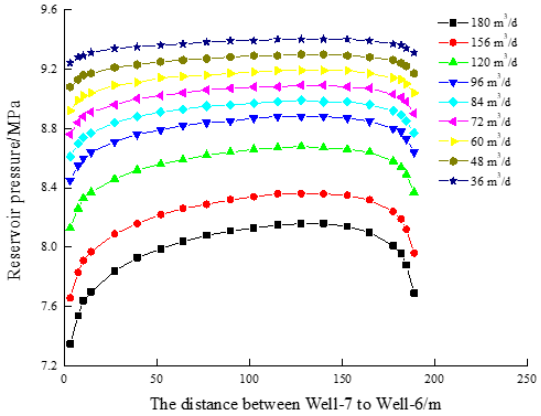

Fig. 7 The pressure distribution from Well-7 to Well-6 at different drainage rates after 20 days production

failure in the late production. The reservoir skeleton compresses rapidly and the permeability decreases fast because of the high drainage rate.

For being convenient to study the reservoir pressure distribution, the points on the line between Well-7 and Well-6 are the research objects. The distance between Well-7 and Well-6 is 188.6 m. Fig. 7 shows the pressure distribution from Well-7 to Well-6 at different drainage rates after 20 days production. From the figure, we know that the pressures of the points decrease with increasing drainage rate. The pressures are the lowest and the speed of pressure drop is the fastest when it has the largest drainage rate (180 m^3/d). Increasing drainage rate results in decreasing

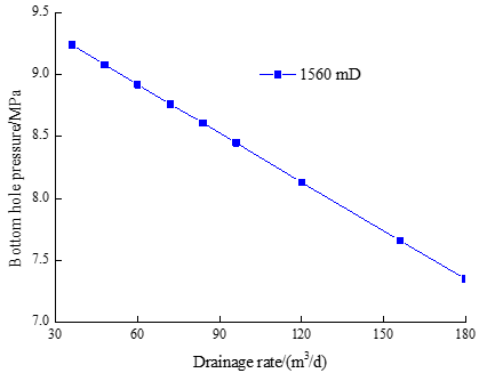

Fig. 8 The relationship between bottom hole pressure and drainage rate after 20 days production

reservoir pressure and bottom-hole pressure, especially the latter. The pressures near the wellbore are influenced most by the drainage rate. Lower flowing bottom-hole pressure may lead to the casing damage, so optimization calculation should be carried out to select the best drainage speed. Based on the field test, the drainage rate of 96 m^3/d can both satisfy the pressure drop speed and prevent casing damage to make water drainage proceed smoothly.

Fig. 8 is the relationship plot between bottom hole pressure and drainage rate when reservoir permeability is 1560 mD. The bottom hole pressure decreases approximately linearly as the drainage rate rises. For example, the bottom hole pressures are respectively 9.24 MPa and 7.35 MPa when the drainage rates are 36 m^3/d and 180 m^3/d after 20 days production. The function relation between them is as follows.

$$P = 9.6 - 13.13 \times 10^{-3} q \tag{15}$$

where P is the bottom hole pressure, MPa; q is the drainage rate of a single well, m^3/d.

3.2.2 Effect of formation permeability on reservoir pressure

To study the effect of the formation permeability on the reservoir pressure distribution, formation permeabilities valued as 496, 851, 1206, 1560, 1915, 2270, 2624 and 2980 mD are simulated. The mining time is 20 days. The other parameters are valued as listed in Table 1.

In this section, Well-7 is set as the research objects. Fig. 9 gives the bottom hole flowing pressure of Well-7 at different permeabilities. Known from the figure, the bottom hole pressure is proportional to the permeability in the case of the fixed drainage rate. The two parameters present the exponential relationship. The permeability has a significant effect on bottom hole pressure when its value is low, especially when the drainage rate is high. As the liquid is produced from the formation, the pressure supported by the fluid is gradually reduced and the reduced pressure is transferred to the solid particles. As the reduced pressure increases, the gap between the particles is constantly compressed. At the macro level, when the bottom hole pressure is constant, the drainage rate is decreasing. The drainage rate is decreasing when the bottom hole pressure is a constant in the actual operation.

The functional relations between bottom hole pressure

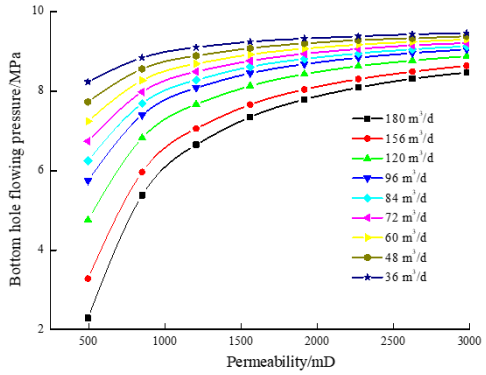

Fig. 9 The relation curve between bottom hole pressure and permeability after 20 days production

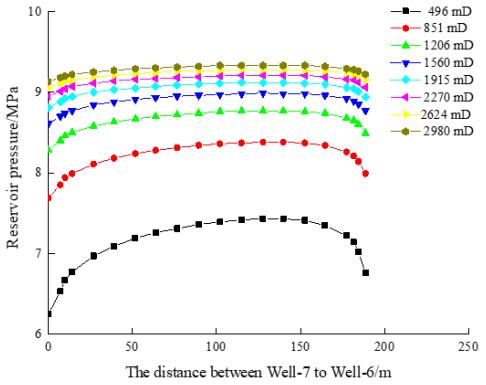

Fig. 10 The pressure distribution from Well-7 to Well-6 at different permeabilities after 20 days production

and permeability are shown as follows

(1) The drainage rate of 84 m^3/d

$$P = 2.24668 + 0.01142K - 7.85408\times10^{-6}K^2 + 2.47544\times10^{-9}K^3 - 2.90524\times10^{-13}K^4 \quad (16)$$

(2) The drainage rate of 96 m^3/d

$$P = 1.13497 + 0.01318K - 9.09896\times10^{-6}K^2 + 2.87619\times10^{-9}K^3 - 3.3826\times10^{-13}K^4 \quad (17)$$

(3) The drainage rate of 120 m^3/d

$$P = -0.98079 + 0.01638K - 1.12975\times10^{-5}K^2 + 3.57145\times10^{-9}K^3 - 4.20559\times10^{-13}K^4 \quad (18)$$

(4) The drainage rate of 180 m^3/d

$$P = -6.32928 + 0.02461K - 1.169809\times10^{-5}K^2 + 5.37209\times10^{-9}K^3 - 6.32944\times10^{-13}K^4 \quad (19)$$

where K is the permeability, $10^{-3}\mu m$.

Fig. 10 shows the pressure distribution between Well-7 and Well-6 at different permeabilities when the drainage rate is the constant of 84 m^3/d. From the figure, we know that the pressures of the points are in proportion to the permeability. The reservoir pressure increases as the permeability rises. Meanwhile, the effect of the hole suction effect decreases with the increase of permeability in the same range. As the permeability increases, the reservoir pressure difference between the two wells reduces greatly. For example, the pressures of Well-7, Well-6 and the maximum value are 9.13 MPa, 9.22 MPa and 9.33 MPa respectively, when the permeability is 2980 mD. The maximum reservoir pressure difference is 0.20 MPa. When the permeability is 496 mD, the pressures of Well-7, Well-6 and the maximum value are 6.25 MPa, 6.76 MPa and 7.43 MPa respectively. At this time, the maximum reservoir pressure difference is 1.18 MPa which is nearly 5.9 times larger than the former.

4. Conclusions

The paper has established the reservoir pressure distribution model, and the numerical simulation model is based to study the distribution law and influencing factors of pressure field distribution before thermal recovery technology in Gudao oilfield. The following conclusions can be drawn.

• The reservoir pressure drops most at the wellbore. The farther the distance away from the borehole, the sparser the isobaric lines distribute. The reservoir pressure of the whole area declines over time, and the pressure difference of the whole research region decreases greatly. The descent velocity of reservoir pressure is faster in the early stage while it becomes slow in the middle and late stage.

• The reservoir pressure decreases with increasing drainage rate. Increasing drainage rate results in decreasing reservoir pressure and bottom-hole pressure, especially the latter. The pressures near the wellbore are most influenced by the drainage rate. Lower flowing bottomhole pressure may lead to the casing damage.

• When reservoir permeability is 1560 mD, the bottom hole pressure decreases approximately linearly as the drainage rate rises. The function relation between them is : $P = 9.6 - 13.13 \times 10^{-3}q$.

• The permeability has a significant effect on bottom hole pressure when its value is low, especially when the drainage rate is high. The bottom hole pressure increases with increasing permeability, however the growth rate decreases gradually. The effect of the hole suction effect decreases with the increase of permeability.

•Based on the field test, the drainage rate of 96 m^3/d can both satisfy the pressure drop speed and prevent casing damage to make water drainage proceed smoothly.

Acknowledgments

This research described in this paper was financially supported by the National Natural Science Foundation of China (Grant No. 51804236), Zhejiang Public Welfare Technology Research Project (LGF18E080004), Special Fund for Basic Scientific Research of Central Public Research Institutes (CKSF2017012/YT).

References

Amirian, E., Dejam, M. and Chen, Z.X. (2018a), “Performance

forecasting for polymer flooding in heavy oil reservoirs", *Fuel*, **216**, 83-100. https://doi.org/10.1016/j.fuel.2017.11.110.

Amirian, E., Fedutenko, E., Yang, C., Chen, Z. and Nghiem, L. (2018b), "Artificial neural network modeling and forecasting of oil reservoir performance", *Appl. Data Manage. Anal.*, 43-67. https://doi.org/10.1007/978-3-319-95810-1_5.

Amirian, E., Leung, J. Y., Zanon, S. and Dzurman, P. (2015), "Integrated cluster analysis and artificial neural network modeling for steam-assisted gravity drainage performance prediction in heterogeneous reservoirs", *Expert Syst. Appl.*, **42**(2), 723-740. https://doi.org/10.1016/j.eswa.2014.08.034.

Arciniegas, L.M. and Babadagli, T. (2014), "Quantitative and visual characterization of asphaltenic components of heavy-oil after solvent interaction at different temperatures and pressures", *Fluid Phase Equilibr.*, **366**, 74-87. https://doi.org/10.1016/j.fluid.2014.01.006.

Bader, A., Hartwich, M., Richter, A. and Meyer, B. (2018), "Numerical and experimental study of heavy oil gasification in an entrained-flow reactor and the impact of the burner concept", *Fuel Process. Technol.*, **169**, 58-70. https://doi.org/10.1016/j.fuproc.2017.09.003.

Cavicchio, C.A.M., Biazussi, J.L., de Castro, M.S., Bannwart, A.C., Rodriguez, O.M.H. and de Carvalho, C.H.M. (2018), "Experimental study of viscosity effects on heavy crude oil-water core annular flow pattern", *Exp. Therm. Fluid Sci.*, **92**, 270-285. https://doi.org/10.1016/j.expthermflusci.2017.11.027.

Deshamukhya, T., Hazarika, S.A., Bhanja, D. and Nath, S. (2019), "An optimization study to investigate non-linearity in thermal behaviour of porous fin having temperature dependent internal heat generation with and without tip loss", *Commun. Nonlin. Sci. Numer. Simul.*, **67**, 351-365. https://doi.org/10.1016/j.cnsns.2018.07.024.

Doranehgard, M.H. and Slavashi, M. (2018), "The effect of temperature dependent relative permeability on heavy oil recovery during hot water injection process using streamline-based simulation", *Appl. Therm. Eng.*, **129**, 106-116. https://doi.org/10.1016/j.applthermaleng.2017.10.002.

Hasanvand, M.Z., Behbahani, R.M., Feyzi, F. and Mousavi-Dehghani, S. (2017), "Asphaltene particles size and size distribution change at high pressure high temperature conditions: experimental study on a heavy oil sample", *High Temp.-High Press.*, **46**(2), 85-99.

Inarrea, M., Lanchares, V., Palaclan, J.F., Pascual, A.I., Salas, J.P. and Yanguas, P. (2019), "Effects of a soft-core coulomb potential on the dynamics of a hydrogen atom near a metal surface", *Commun. Nonlin. Sci. Numer. Simul.*, **68**, 94-105. https://doi.org/10.1016/j.cnsns.2018.07.039.

Jahani-Keleshteri, Z. and Bahadori, A. (2017), "An accurate model to predict viscosity of heavy oils", *Petrol. Sci. Technol.*, **35**(4), 371-376. https://doi.org/10.1080/10916466.2016.1259632.

Jiang, T.T., Zhang, J.H. and Wu, H. (2017), "Effects of fractures on the well production in a coalbed methane reservoir", *Arab. J. Geosci.*, **10**(22), 494. https://doi.org/10.1007/s12517-017-3283-7.

Kim, P.C., Lloyd, J., Kim, J.W., Abdoulmoumine, N. and Labbe, N. (2016), "Recovery of creosote from used railroad ties by thermal desorption", *Energy*, **111**, 226-236. https://doi.org/10.1016/j.energy.2016.05.117.

Kumar, G.S. and Reddy, D.S. (2017), "Numerical modelling of forward in-situ combustion process in heavy oil reservoirs", *Int. J. Oil Gas Coal T.*, **16**(1), 43-58. https://doi.org/10.1504/IJOGCT.2017.10006351.

Kumar, A. and Okuno, R. (2015), "Direct perturbation of the Peng-Robinson attraction and covolume parameters for reservoir fluid characterization", *Chem. Eng. Sci.*, **127**, 293-309. https://doi.org/10.1016/j.ces.2015.01.032.

Kurek, M.A., Moczkowska, M., Pieczykolan, E. and Sobieralska, M. (2018), "Barley beta-d-glucan-modified starch complex as potential encapsulation agent for fish oil", *Int. J. Biol. Macromol.*, **120**(Pt A), 596-602. https://doi.org/10.1016/j.ijbiomac.2018.08.131.

Mahdavi, A., Medvedovski, E., Mendoza, G.L. and McDonald, A. (2018), "Corrosion resistance of boronized, aluminized, and chromized thermal diffusion-coated steels in simulated high-temperature recovery boiler conditions", *Coatings*, **8**(8), 257. https://doi.org/10.3390/coatings8080257.

Osgouei, Y.T. and Parlaktuna, M. (2018), "Effects of minerals on steam distillation during thermal heavy-oil recovery: An experimental investigation", *Energy Source. Part A*, **40**(6), 662-672. https://doi.org/10.1080/15567036.2018.1454547.

Oskouel, S.J.P., Zadeh, A.B. and Gates, I.D. (2017), "A new kinetic model for non-equilibrium dissolved gas ex-solution from static heavy oil", *Fuel*, **204**, 12-22. https://doi.org/10.1016/j.fuel.2017.05.018.

Riazi, N., Lines, L. and Russell, B. (2015), "Monitoring heavy oil recovery by time-lapse EEI inversion", *J. Seism. Explor.*, **24**(4), 343-364.

Rostami, B., Pourafshary, P., Fathollahi, A., Yassin, M.R., Hassani, K., Khosravi, M., Mohammadifard, M. and Dangkooban, A. (2017), "A new approach to characterize the performance of heavy oil recovery due to various gas injection", *Int. J. Multiphas. Flow*, **99**, 273-283. https://doi.org/10.1016/j.ijmultiphaseflow.2017.10.014.

Salmo, I.C., Pettersen, O. and Skauge, A. (2017), "Polymer flooding at an adverse mobility ratio: Acceleration of oil production by crossflow into water channels", *Energy Fuel.*, **31**(6), 5948-5958. https://doi.org/10.1021/acs.energyfuels.7b00515.

Shalaby, R.M., Kamal, M., Ali, E.A.M. and Gumaan, M.S. (2017), "Microstructural and mechanical characterization of melt spun process Sn-3.5Ag and Sn-3.5Ag-xCu lead-free solders for low cost electronic assembly", *Mater. Sci. Eng. A Struct.*, **690**, 446-452. https://doi.org/10.1016/j.msea.2017.03.022.

Taghizadeh, R., Goshtasbi, K., Manshad, A.K. and Ahangari, K. (2018), "Geomechanical and thermal reservoir simulation during steam flooding", *Struct. Eng. Mech.*, **66**(4), 505-513. https://doi.org/10.12989/sem.2018.66.4.505.

Wang, T.T., Li, J.J., Jing, G., Zhang, Q.Q., Yang, C.H. and Daemen, J.J.K. (2019), "Determination of the maximum allowable operating pressure for a gas storage underground salt cavern–A case study of Jintan, China", *J. Rock Mech. Geotech. Eng.*, **11**(2), 251-262. https://doi.org/10.1016/j.jrmge.2018.10.004.

Wang, T.T., Yang, C.H., Wang, H.M., Ding, S.L. and Daemen, J.J.K. (2018a), "Debrining prediction of a salt cavern used for compressed air energy storage", *Energy*, **147**, 464-476. https://doi.org/10.1016/j.energy.2018.01.071.

Wang, T.T., Ding, S.L., Wang, H.M., Yang, C.H., Shi, X.L., Ma, H.L. and Daemen, J.J.K. (2018b), "Mathematic modelling of the debrining for a salt cavern gas storage", *J. Nat. Gas Sci. Eng.*, **50**, 205-214. https://doi.org/10.1016/j.jngse.2017.12.006.

Wang, T.T., Yang, C.H., Chen J.S. and Daemen, J.J.K. (2018c), "Geomechanical investigation of roof failure of China's first gas storage salt cavern", *Eng. Geol.*, **243**, 59-69. https://doi.org/10.1016/j.enggeo.2018.06.013.

Wang, T.T., Ma, H.L., Shi, X.L., Yang, C.H., Zhang, N., Li, J.L., Ding, S.L. and Daemen, J.J.K. (2018d), "Salt cavern gas storage in an ultra-deep formation in Hubei, China", *Int. J. Rock Mech. Min. Sci.*, **102**, 57-70. https://doi.org/10.1016/j.ijrmms.2017.12.001.

Ziabakhsh-Ganji, Z., Nick, H.M., Donselaar, M.E. and Bruhn, D.F. (2017), "Synergy potential for oil and geothermal energy exploitation", *Appl. Energy*, **212**, 1433-1447. https://doi.org/10.1016/j.apenergy.2017.12.113.

Zhang, C.Y., Pu, C.Z., Cao, R.H., Jiang, T.T. and Huang, G. (2019), "The stability and roof-support optimization of roadways passing through unfavorable geological bodies using advanced detection and monitoring methods, among others, in the Sanmenxia Bauxite Mine in China's Henan Province", *Bull. Eng. Geol. Environ.*, 1-13, https://doi.org/10.1007/s10064-018-01439-1.

CC